Measurement of the ^{237}Np(n, γ) cross section from 20 meV to 500 keV with a high efficiency, highly segmented 4π BaF_2 detector

E.-I. Esch,[1,*] R. Reifarth,[1,2,†] E. M. Bond,[1] T. A. Bredeweg,[1] A. Couture,[1] S. E. Glover,[1] U. Greife,[2] R. C. Haight,[1] A. M. Hatarik,[2] R. Hatarik,[2,‡] M. Jandel,[1] T. Kawano,[1] A. Mertz,[1,§] J. M. O'Donnell,[1] R. S. Rundberg,[1] J. M. Schwantes,[1,‖] J. L. Ullmann,[1] D. J. Vieira,[1] J. B. Wilhelmy,[1] and J. M. Wouters[1]

[1]*Los Alamos National Laboratory, Los Alamos, New Mexico 87545, USA*

[2]*Colorado School of Mines, Golden, Colorado 80401, USA*

(Received 23 March 2007; revised manuscript received 15 January 2008; published 18 March 2008)

The ^{237}Np$(n, \gamma)^{238}$Np cross section has been measured in the neutron energy range from 20 meV to 500 keV using the DANCE array at the Los Alamos National Laboratory. This new facility allows experiments with submilligram samples and is therefore well suited to investigate isotopes with half-lives as low as a few hundred days. In this benchmark measurement, only 0.42 mg of ^{237}Np was sufficient to determine differential cross sections relative to the well-known resonance at 0.5 eV. The thermal cross section was measured to $\sigma_{2200\,\mathrm{m/s}} = 177 \pm 5$ barn, $\sigma_{kT=25.3\ \mathrm{meV}} = 167 \pm 4$ barn and the resonance integral to $RI = 693 \pm 6$ barn.

DOI: 10.1103/PhysRevC.77.034309 PACS number(s): 25.40.Lw, 29.40.Vj, 29.25.Dz, 29.40.Wk

I. INTRODUCTION

^{237}Np is a major constituent of spent nuclear fuel. Estimates place the amount of ^{237}Np bound for the Yucca Mountain high-level waste repository at 40 metric tons. The Department of Energy's (DOE) Advanced Fuel Cycle Initiative (AFCI) is evaluating methods for transmuting the actinide waste from commercial nuclear power plants. The critical parameter that defines the transmutation efficiency of actinide isotopes is the neutron fission-to-capture ratio for the particular isotope in a given neutron spectrum. The calculation of transmutation efficiency therefore requires accurate fission and capture cross sections [1]. Current ^{237}Np evaluations available for transmuter system studies show significant discrepancies in both the fission and capture cross sections in the energy regions of interest. So far, there are data from two types of experiments investigating the neutron capture branch, activation experiments and time-of-flight (TOF) experiments. The main handicap of the activation experiments is the fact that ^{237}Np(n, γ) has a huge resonance at 0.49 eV, which disturbs the cadmium difference method, since the Cd-cut-off is affected by this resonance. Furthermore, the recommended value for the γ-ray intensity of the prominent 984 keV line of the ^{238}Np decay has significantly changed from the value used by the authors [2–8]. All of the TOF experiments had to use samples of at least one gram, which made significant corrections for multiple scattering and self absorption necessary. Apart from that, the background due to scattered neutrons is typically not at all discussed in the papers [9–13]. New preliminary data have been reported from the n-TOF collaboration [14].

Since the DANCE array at the Los Alamos National Laboratory allows differential neutron capture cross section measurements between 10 meV and about 500 keV, the discrepancies could be resolved with an independent measurement using a different approach.

II. EXPERIMENT

A. The DANCE array

The Detector for Advanced Neutron Capture Experiments (DANCE) is designed as a high efficiency, highly segmented 4π-BaF_2 detector for calorimetrically detecting γ-rays following a neutron capture. This allows the disentanglement of captures on different isotopes based on their reaction Q-value, the sum of all γ-ray energies emitted. DANCE is located on a 20 m neutron flight path (FP14) at the Manuel Lujan Jr. Neutron Scattering Center at the Los Alamos Neutron Science Center (LANSCE) [15]. The neutron flux at the sample position is 3×10^5 n/s/cm^2/decade. The initial design work is described in [16]. For practical reasons the detector modules do not cover the entire solid angle. The design of the detector is such that a full 4π array would consist of 162 crystals of four different shapes, each shape covering the same solid angle [17]. Two of the 162 crystals are left out in order to leave space for the neutron beam pipe. Thus the full array hosts 160 out of 162 possible BaF_2 crystals. The dimensions of the bare crystals are designed to form a BaF_2 shell with an inner radius of 17 cm and a thickness of 15 cm. In reality the crystals had to be moved outwards by 1 cm in order to leave space for wrapping. Together with the fact that only 160 crystals can be used, the actual solid angle covered by the detector is reduced from 4π to about 3.6π. The high granularity of the array has two main advantages. First, the potentially high count rate is distributed over several crystals and pile-up problems are therefore less pronounced. The second advantage is that

*ernst@lanl.gov

†Present affiliation: Gesellschaft für Schwerionenforschung mbH, Darmstadt, D-64291, Germany.

‡Present affiliation: Rutgers University, New Brunswick, New Jersey 08901, USA.

§Present affiliation: Department of Physics, Yale University, New Haven, CT 06520, USA.

‖Present affiliation: Pacific Northwest National Laboratory, Richland, Washington 99352, USA.

different components of the signal yield different multiplicity distributions. Neutron capture events on the sample tend to yield higher multiplicities than capture events of scattered neutrons or radioactive decays [16,18].

This information can therefore be used to improve the signal-to-background ratio. Further details can be found in section III C of this article. Thanks to the fairly low repetition rate of 20 Hz, measurements can in principle be carried out over the whole energy range from 10 meV to 500 keV. This combination of a strong neutron source and a high efficiency γ-ray detector allows measurements of (n, γ) cross sections on submilligram size samples, enabling experiments with radioactive isotopes down to a few hundred days half-life. Further details on the overall performance of the array can be found in [18,19].

B. The neptunium target

The ^{237}Np target was manufactured by the Isotope and Nuclear Chemistry group at Los Alamos National Laboratory. The ^{237}Np was first chemically separated from its decay daughter ^{233}Pa using anion-exchange column chemistry and then electro-plated out of an ammonium sulfate solution onto two 2 μm thick Ti foils [20].

The foils were assayed by quantitative α-counting before they were glued together with the ^{237}Np deposits facing each other and re-assayed well after the experiment via γ-counting. Epoxy was used around the edge of the 25 mm square Ti foils with small pathways left open for pump out. For second containment the target was mounted in the center of an aluminum cylinder (5 cm long, 4.2 cm diameter) with 50 μm thick Kapton entrance and exit windows [21]. The impact of such Kapton windows on the background caused by scattered neutrons is discussed in [18]. This target assembly was then placed in the center of the DANCE array to perform the neutron capture measurement. The total amount of ^{237}Np was determined to be $(1.06 \pm 0.03) \times 10^{18}$ atoms corresponding to 0.42 ± 0.01 mg deposited with a diameter of 6.4 mm. The chemical purity was better than 99%.

C. The neutron flux at DANCE

The energy dependence of the neutron flux was determined using ^{197}Au data from DANCE and neutron monitor data taken downstream of the DANCE array. A gold foil of 0.01 mm thickness (20 mg/cm^2) was placed in the center of the DANCE array in the standard sample position. The gold data were taken for the thermal regions and for the energy region above 1 keV. Since the neutron cross section of gold varies over many orders of magnitude in the resolved energy region between 1 eV and $\approx$500 eV, it is not suited for neutron monitoring in this energy region. Instead the well known ^{6}Li$(n, \alpha)t$ and ^{10}B$(n, \alpha)^7$Li reactions were used as the flux-monitoring reaction. For that purpose, an aluminum foil with a deposit of enriched ^{6}LiF was placed downstream of the DANCE array. A silicon surface barrier detector was used to detect the emitted alphas and tritons from the ^{6}Li$(n, \alpha)\,t$ reaction. The ^{10}B$(n, \alpha)^7$Li reaction was detected with a commercially available BF_3 detector from

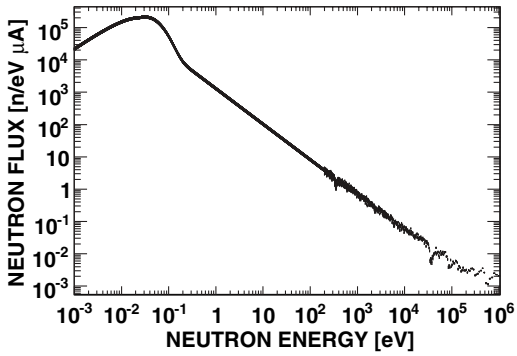

FIG. 1. The neutron flux at FP14. The neutron flux given per μA and typically 100 μA of beam are available during the experiment.

LND, Inc. (LND 2231). The neutron flux normalized to the proton current is given in Fig. 1. The LANSCE accelerator typically delivers 100 μA to the Lujan Center.

The diameter of the neutron beam is approximately 1 cm (FWHM) and is homogeneous over the in inner 0.6 cm. This was determined with two methods—image plates and a set of gold foils of different diameters, see [22] for details. The diameters of the beam and sample are similar, which makes it difficult to determine the exact number of neutrons passing through the sample. Therefore we decided to make this measurement relative to an energy region, where the cross section is well known. If such an approach would not be possible for other isotopes, since no other data are available, the sample size should be chosen either significantly bigger, or smaller than the beam.

D. Data acquisition

The BaF_2 signals were digitized for software preprocessing using 320 channels of Acqiris model DC265 transient digitizers (Agilent Tecnologies SA, Geneva, Switzerland). The DC265 has a maximum sampling rate of 500 MS/s (million samples per second), or 2 ns per sample. The configuration for DANCE has a dedicated storage capacity of 128 kS per channel. The digitizer cards were mounted in fourteen Acqiris model CC108 CompactPCI crates, consisting of six digitizer cards plus one single board computer for digitizer control and readout per crate. One Acqiris crate supports twelve detectors, since each detector signal was split into high and low gain channels. The total available memory per channel can be configured as a single contiguous block (up to 250 μs), or as several smaller regions of memory, each of which can store a single acquired waveform. In the latter case it is possible to perform several independent "sequential" acquisitions, each with its own associated trigger, before stopping the acquisition to read out the stored waveforms. Memory and processing limitations, as well as dead-time and total run time concerns eventually lead to the development of two distinct operating modes based on these two extremes. These two modes are aptly named continuous mode (one trigger per neutron spill) and segmented mode (one trigger per signal). During the ^{237}Np experiment the neutron energy range from 10 meV to 10 keV was investigated with the segmented mode and the energy

range above 260 eV with the continuous mode. It was therefore possible to normalize the two data sets in the overlapping region between 260 eV and 10 keV to measure the entire cross section relative to the well known resonance at 0.49 eV.

1. Low energies—segmented mode

The so-called segmented mode of the data acquisition was used to cover up to 14 ms of neutron time of flight after the γ-flash, which is produced when the protons hit the tungsten spallation target. This corresponds to neutron energies greater than 11 meV. As explained above, the total available memory of 128 KS per channel was divided into segments of 1000 samples, or 2 μs. As soon as two of the 160 detectors showed an energy deposition of more than 100 keV, the data acquisition of the corresponding detectors was triggered. No additional trigger was allowed for 3 μs after that, which ensured that all 160 channels were ready to accept data for the next trigger. The 3 μs dead time was necessary, because in addition to the 2 μs looking time, approximately 0.9 μs is required to arm a new segment in the Acqiris digitizers. The neutron scattering cross section of ^{237}Np is smaller than the capture cross section for neutron energies below 1 keV. The equation for the count rate estimate given in [18] can therefore be applied. If the (n,γ) cross section is $\sigma(E) = c/\sqrt{E}$ and N_{sample} is the number of sample atoms, the instantaneous neutron capture rate at any time during the duration of the neutron pulse would be

$$\frac{dC}{dt} = \frac{d\Phi}{dE}\cdot\frac{dE}{dt}\cdot\sigma(E)\cdot N_{\text{sample}} = 2.7\times10^{8}\cdot c\cdot N_{\text{sample}}\frac{1}{\sqrt{\text{keV}}\,\text{s}\,\text{cm}^2}.$$

Inserting the values for the ^{237}Np experiment of 2 kbarn at the top of the resonance at 0.5 eV gives $c = 3.510^{-22}\text{cm}^2\sqrt{\text{keV}}$. The sample mass was 0.42 mg, or $N_{\text{sample}} = 1.06\times10^{18}$, resulting in an upper limit for maximum instantaneous neutron capture rate of 4×10^{4} s^{-1}, or one capture every 25 μs. The actual count rate during the experiment was significantly lower, mostly because of the fact that the accelerator was not operating at 100 μA and the sample was not entirely covered by the beam. A careful analysis of the dead-time corrections necessary revealed that the dead time corrections are very small at the peak of the strongest resonance and entirely negligible elsewhere. This picture changes entirely for neutron energies above 10 keV. Since the most dominant reaction is neutron scattering, which does not decrease as much as neutron capture with increasing neutron energies, the instantaneous count rate at high energies is greater than in the estimate given above. This implies the need for the continuous data acquisition mode, since the segmented mode suffers severely from the fixed dead time of 3 μs. Approximately one day of beam time was spent in the segmented mode with looking times of 10 or 14 ms. One additional day was spent on calibration and background runs. At this low energy, the background in the region of interest around the Q-value of the ^{237}Np(n,γ) reaction was determined by neutron scattering by the Kapton window and the titanium foil. The only sample-related background component—neutron scattering off neptunium is much smaller, because of the much smaller number of neptunium atoms in the beam. The background runs were therefore taken with a blank target holder containing two titanium foils—basically the sample without neptunium in the beam.

2. High energies—continuous mode

The neutron energies above 260 eV were investigated with the so-called continuous mode data acquisition. The main advantage is that this mode allows much higher instantaneous data rates than the segmented mode. There are two reasons for this. First, the continuous mode works on a crystal-by-crystal basis. That means that the dead-time in one crystal is not influenced by counts in another crystal. Considering an average crystal multiplicity of five for neutron-induced events, an increased count rate of a factor of 32 can be handled. Second, since this mode takes data continuously for 100 μs, the highest possible count rate is mainly determined by the desired coincidence window and not by the fact that the data acquisition needs to be stopped for a certain time in order to be armed for the next event. This enables us to to use a pile-up correction for the data instead of just the data rejection required in the segmented mode, resulting in an increased rate of at least a factor of 30. Altogether, the continuous mode is able to handle up to three orders of magnitude higher count rate. Dead time corrections were therefore not necessary in the continuous mode. The data acquisition in the continuous mode allowed presampling, which means that the beginning of the actual data can be up to one segment length (100 μs in this case) before the trigger. The trigger in the Lujan Center is a pick-up signal from the proton beam. We used the presampling feature to take 10 μs worth of data before the proton pulse hits the tungsten target, which allows investigation of the nonbeam related background. The remaining 90 μs looking time correspond to neutron energies of 260 eV and above, see Fig. 2.

Neutron capture cross sections in the keV-region are generally much smaller than at thermal energies, while the background reactions, such as scattering often have similar values in both regions. This implies the need for more beam time in the higher energy regime. Approximately four days of beam time were spent in the continuous mode irradiating the neptunium sample. An additional three days were spent on

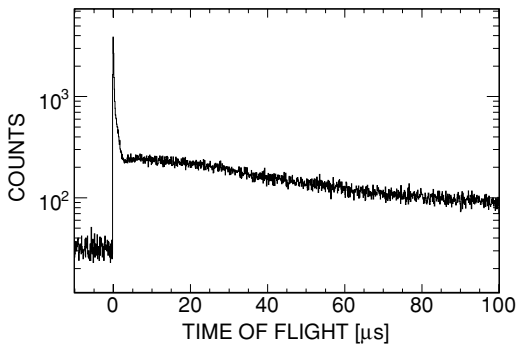

FIG. 2. Typical time-of-flight spectrum at DANCE without further cuts. The sharp peak at time 0 corresponds to the γ-flash. Events before the γ-flash are mostly non-beam-related.

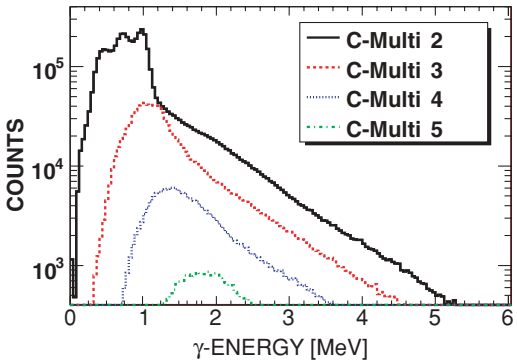

FIG. 3. (Color online) Sum-energy spectra of different cluster multiplicities (see text) for a lead sample inside DANCE with a 1.25 cm polyethylene block upstream of the sample. Since most of the neutrons are scattered out of the beam, the remaining spectrum corresponds to interactions of γ-rays with the sample. The pronounced peak at 1 MeV originates from pair production at the lead sample. The spectrum corresponds to neutron energies above 30 eV.

different background runs. At the higher energies investigated with the continuous mode, neutron scattering off the backing and housing materials is not the only important background component—in contrast to the late times investigated with the segmented mode. Especially for times of flight less than 10 μs after the γ-flash (neutron energies above 20 keV), interactions of γ-rays with the material in the beam are significant. These γ-rays originate from neutron captures on upstream material, such as the water moderator or stainless steel and aluminum windows [18]. Since the total interaction probability for photons increases rapidly with the charge of the nucleus for γ-rays, the contribution due to the neptunium atoms is no longer negligible. In order to subtract the contribution of this background component in the energy region of interest, a spectrum from a lead run with a 1.25 cm thick polyethylene filter between the neutron production target and the sample was analyzed. Such a filter scatters more than 90% of the neutrons out of the beam, while it is more than 90% transparent for gammas above 1 MeV. The lead spectrum was normalized at the 1 MeV peak in the sum energy spectrum and subtracted from the neptunium data after the contribution from an empty radioactive target holder (RTH) with titanium foils was subtracted. Figure 3 shows the sum energy spectrum of the lead run summed over detector cluster multiplicities 2–5 (the meaning of cluster multiplicities will be discussed in the next section). The pronounced peak at 1 MeV is a direct result of photon pair production—the most important interaction mechanism for high energy photons. Above that peak, there is no feature in the quickly declining spectrum. This is expected based simulations carried out with GEANT 3.21 [18,23]. It proves the assumption that the polyethylene filter clears the beam off neutrons. The corrections in the region of the Q-value peak of the ^{237}Np(n,γ) reactions were always below 5%.

III. DATA ANALYSIS

The data analysis was split up into two branches and several steps so that it was possible to retrace the work and commit to changes in a timely manner. The two branches in the analysis represent the data from the continuous mode and the segmented mode. It was necessary to analyze these two measurements separately since they had different run-times and needed to be normalized to the measured neutron flux during the experiment. Once a cross section yield was calculated for both data sets, the two analysis branches were united and the cross section was determined.

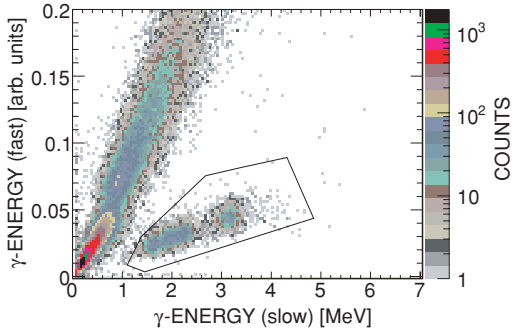

FIG. 4. (Color online) 2D particle identification plot for crystal 0 using segmented mode. During the segmented mode neither fast nor slow component are saturated and all γ-ray induced events as well as α-events are on two separated lines. The α-particle cut is indicated by the black lines inside the figure.

A. Intrinsic detector background

The BaF_2 crystals have an intrinsic background that originates from radium in the crystal. Because of its chemical similarity to barium, radium cannot be completely separated out of the crystal material. Therefore, radium and its daughters generate an alpha background in the detectors. In contrast to γ-rays, α-particles do not produce a fast component when they are stopped in the BaF_2 crystals. By using a two-dimensional plot of fast integral versus slow integral, it is possible to generate a particle identification and remove the α-decay background from the data on a crystal-by-crystal base (see Figs. 4 and 5). Figure 6 shows the isolated α-event energy in arbitrary units. Overlaid over the data is the fit used to perform

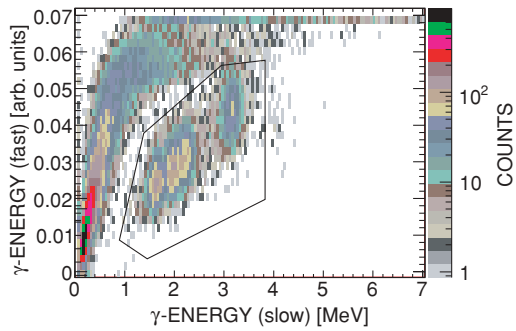

FIG. 5. (Color online) 2D particle identification plot for crystal 0 using continuous mode. During the continuous mode the fast component is saturated for γ-rays above 2 MeV. The γ-rays induced events are now on a shaped curve and the α-events are a separated line. The α-particle cut is indicated by the black lines inside the figure.

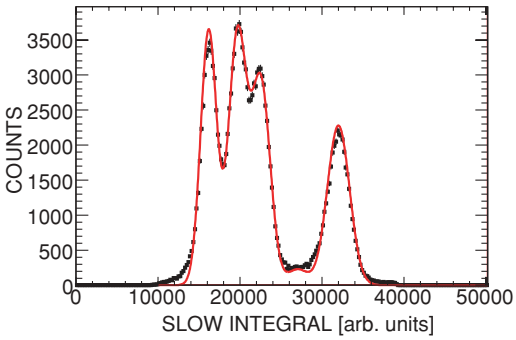

FIG. 6. (Color online) Counts from α-activity in crystal 0 and respective fit used for energy calibration. This histogram contains only events with a particle-ID corresponding to α-decays.

an α-energy calibration. The four dominant lines originate from the α-decays of ^{226}Ra (4.8 MeV), ^{222}Rn (5.5 MeV), ^{218}Po (6.0 MeV), and ^{214}Po (7.7 MeV).

B. Energy calibration of different runs

The initial energy calibration of the detector array was done with standard radioactive sources. Since the data acquisition software was not able to write data into file sizes larger than 2 GB, it was necessary to restart the data acquisition every 4 to 6 h. From the first run to the last run taken, a gain drift of about 15% was observed in the energy spectra of all crystals. In order to compensate for this drift the energy values of each detector for each different run had to be scaled. The shift of the peak positions of the α-decay peaks in the detectors themselves were used to determine the scaling factor. This method was chosen since it provided a γ-ray energy calibration for the ^{237}Np files as well as for the background files. Once the energy calibration was done, a data file with a tree structure was written using the analysis package ROOT [24]. The tree consisted of high and low gain integral (energy) for each detector fired, detector number, number of detectors and number of clusters. A cluster was defined as all detectors that triggered during one event and were neighboring each other. In the continuous mode a software coincidence gate of 100 ns was used to generate the triggers of one event. As an example, Fig. 7 shows the time difference between crystal 2 and crystal 0 for events in which

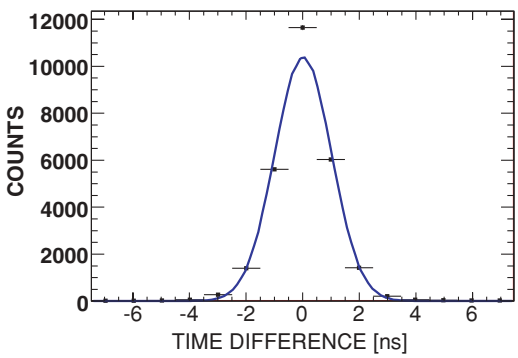

FIG. 7. (Color online) Time difference of crystal 2 relative to crystal 0 and respective fit used for time calibration.

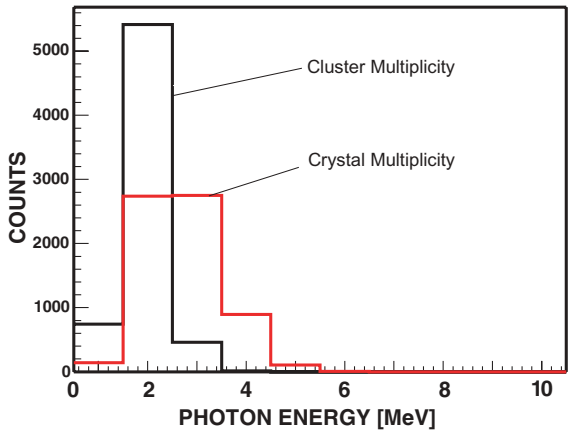

FIG. 8. (Color online) Comparison of cluster vs crystal multiplicity for a ^{88}Y calibration source. Of all decays 94% have γ-multiplicity 2 and most of the remaining decays yield γ-multiplicity 1 [25].

both fired. The fit gives a FWHM of 3.5 ns. The differences for crystals of different cards of the Acquiris modules were bigger, but never exceeded 10 ns FWHM, which means that the 100 ns coincidence window is conservatively wide.

C. Data reduction

The DANCE array is able to separate events based on their multiplicity. Neighboring crystals that fired during an event are combined to one single cluster in order to make corrections for cross-talk. Figure 8 illustrates the advantage of using the cluster multiplicity over crystal multiplicity at the example of the ^{88}Y decay. Obviously the cluster multiplicity is much closer to the emitted γ-ray multiplicity than the crystal multiplicity is. If not otherwise specified, the term multiplicity refers therefore to cluster multiplicity for the remainder of the article. Further details on cluster multiplicities can be found in [16].

Neptunium capture events occur most frequently at cluster multiplicity three, while most of the background events from scattered neutrons yield multiplicities one and two. The best foreground-to-background ratio was found for cluster multiplicities three and four. After subtracting the intrinsic alpha events out of the data, a cluster multiplicity cut for

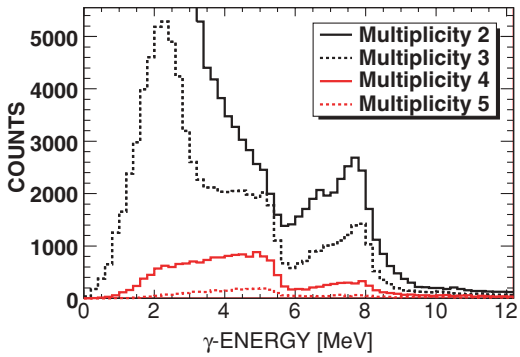

FIG. 9. (Color online) Total energy deposited in the ball as a function of cluster multiplicity for neutron energies between 15 meV and 25 meV.

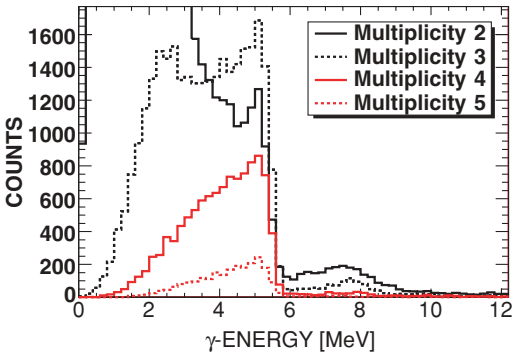

FIG. 10. (Color online) Total energy deposited in the ball as a function of cluster multiplicity for neutron energies between 0.4 eV and 0.6 eV (first resonance).

multiplicities of 3 and 4 was applied and event-by-event the total energy deposition in the ball was collected in an energy histogram. 12000 histograms were generated. Each histogram contained the total energy deposition in the ball for a certain neutron energy range. The neutron energy range was split up into 1000 intervals per decade beginning at 10^{-3} eV. The same cuts were applied to background runs that contained no neptunium, but were otherwise identical to the neptunium setup. Figure 9 shows the total energy deposition in the thermal region. Figure 10 shows the total energy deposition in the first resonance, Fig. 11 shows the energy deposition in the array for the second and third resonance. In each energy region cluster multiplicity of 3 and 4 are dominated by the neptunium capture peak (Q = 5.5 MeV).

The pure Ti-runs were then used for subtracting the background from the Np-signal. The Ti-runs were treated the same way as the Np-runs. A multiplicity cut and a particle-ID cut were applied. The same histograms as with the Np-runs were generated. In order to subtract the two different signals from each other, a Np peak region of interest, ROI(1), was generated between 4.5 MeV and 5.5 MeV total γ-ray energy. A second region of interest, ROI(2), was generated for total detected γ-ray energies between 6.5 MeV and 10 MeV, which is above events expected from ^{237}Np(n,γ) with a Q-value of 5.5 MeV. This second region of interest is dominated by neutron captures on ^{135,137}Ba in the crystals following neutron

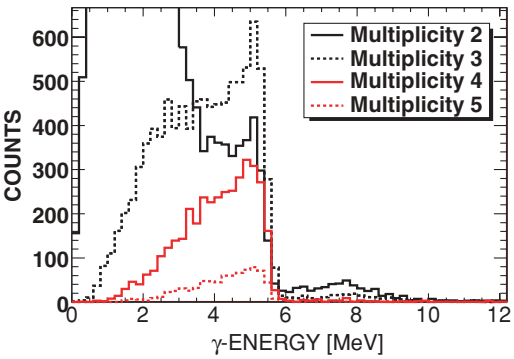

FIG. 11. (Color online) Total energy deposited in the ball as a function of cluster multiplicity for neutron energies between 1.4 eV and 1.6 eV (second and third resonance).

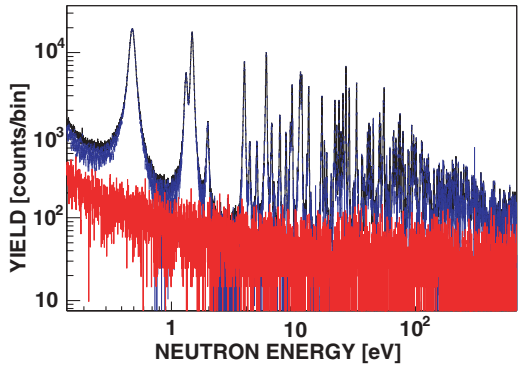

FIG. 12. (Color online) Measured counts (black), ^{237}Np yield (blue), background (red) for low energies. These data were obtained using the segmented mode data acquisition.

scattering off the sample as well as neutron captures on the titanium backing. In order to compensate for the different neutron irradiation doses in the Ti and Np-runs, we investigated the following ratio for each energy histogram at each neutron energy:

$$R(E_{\text{neutron}}) = \frac{\int ROI(2)_{Np}\mathrm{d}E_\gamma}{\int ROI(2)_{Ti}\mathrm{d}E_\gamma}.$$

This ratio was then multiplied by the integral of ROI(1) in the Ti spectrum. The product was then subtracted from the integral of ROI(1) in the Np spectrum.

$$N_{Np}(E_{\text{neutron}}) = \int ROI(1)_{Np}\mathrm{d}E_\gamma - R\int ROI(1)_{Ti}\mathrm{d}E_\gamma.$$

This calculated number represents a neutron capture yield for ^{237}Np at the given neutron energy. Figure 12 displays the measured counts in the ROI(1) for the Neptunium (black), the scaled background (red) and the subtraction (blue). Figure 13 shows the same plot for higher neutron energies. Since the count-rates per eV were lower at higher energies, the bin width was chosen to be 10 bins per energy decade instead of the 1000 bins per decade used at lower energies.

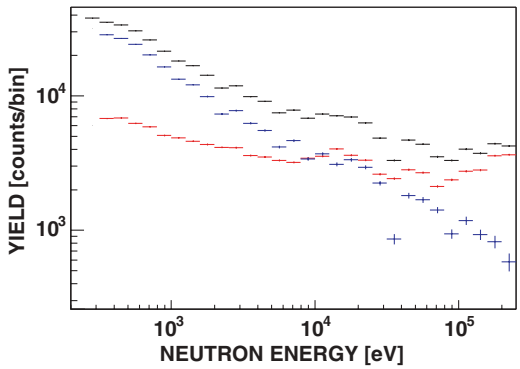

FIG. 13. (Color online) Measured counts (black), ^{237}Np yield (blue), background (red) for high energies. These data were obtained using the continuous mode data acquisition.

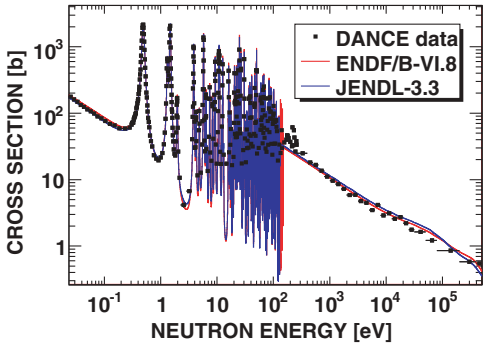

FIG. 14. (Color online) Comparison of the presently measured ^{237}Np(n, γ) cross sections with the data evaluations JENDL-3.3 [26], ENDF/B-VI.8 [27]. Fig. 15 shows the thermal region in more detail, while Figs. 16 and 17 show the resolved and unresolved region.

The two independent analysis branches were combined after the yield was determined by scaling the continuous mode to the segmented mode yield in the overlap region of 260 eV to 1 keV.

IV. RESULTS AND DISCUSSION

A. ^{237}Np(n, γ) cross sections and related uncertainties

In order to significantly reduce the systematic uncertainties, the measured ^{237}Np yield was normalized to the available data evaluations (JENDL-3.3 [26], ENDF/B-VI.8 [27]) in the region of the 0.49 eV resonance. All evaluations agree in this region. A systematic uncertainty at other energies arises from the determination of the neutron flux spectrum, which follows a power law, $\phi_n(E) = \text{const} \cdot E^{\alpha}$, with $\alpha \approx -1$. A fit to the existing flux data results in a systematic uncertainty of 0.5% for α. This gives systematic uncertainties of 5% at the high-energy end of the spectrum and less than 3% for all energies below 1 keV for the extrapolation from the normalization point at 0.5 eV. Figure 14 shows a comparison of the resulting capture cross section data including the statistical uncertainties with evaluations and Figs. 15–17 emphasize the different energy regions. The data are also available online through the Experimental Nuclear Reaction Data (EXFOR) site and the Electronic Physics Auxiliary Publication Service [28].

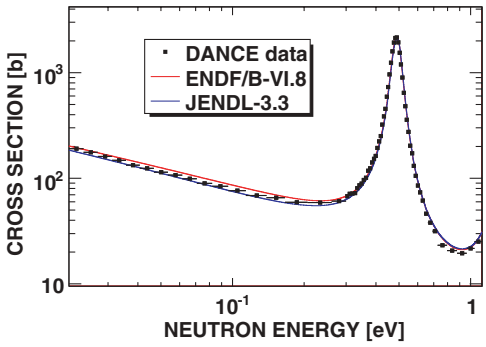

FIG. 15. (Color online) Comparison of the presently measured ^{237}Np(n, γ) cross sections with the data evaluations JENDL-3.3 [26], ENDF/B-VI.8 [27] in the thermal region.

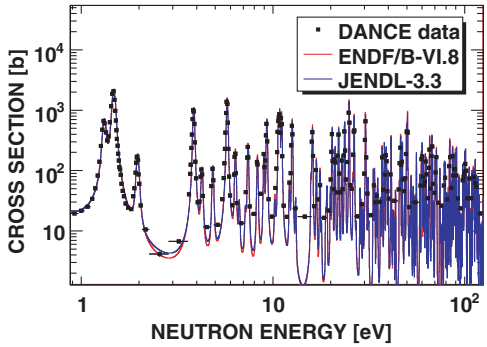

FIG. 16. (Color online) Comparison of the presently measured ^{237}Np cross sections with the data evaluations JENDL-3.3 [26], ENDF/B-VI.8 [27] in the region of resolved resonances.

B. Discussion

These results can be compared with other differential measurements and with integrated values. In the thermal and resolved energy region, our results are consistent with those of Weston [10] Kobayashi [29], see Fig. 18. Because of the beam pulse width and the moderation at LANSCE, our resolution is worse than [10] at higher energies, but better than the data from [29], which result from a lead-slowing-down (LSDS) experiment. In the region from 0.5 to over 100 keV, our values are slightly lower than those of Weston [10] and Kobayashi [29], but are in agreement with high-energy activation data by Lindner [5] (see Fig. 19). The only reported single-shot experiment by Semon [9] shows significantly lower results than all other reported experiments (see Fig. 20). Also the energy dependence of the single-shot experiment deviates from other reported experiments.

A resonance analysis has not been performed, since the main scope of this project was to resolve the inconsistencies in the unresolved resonance region, which is the region of interest for fast reactor applications.

Our value for the capture cross section at 25.3 meV is $\sigma_{2200\,\text{m/s}} = 176.7 \pm 5.0$ barn, the Maxwellian averaged thermal cross section is $\sigma_{kT=25.3\,\text{meV}} = 167.1 \pm 0.3\_\text{stat} \pm 4.4_{\text{syst}}$ barn and the resonance integral above 0.5 eV is $RI = 692.8 \pm 2.3_{\text{stat}} \pm 5.8_{\text{syst}}$ barn. Very comprehensive reviews on the existing experimental data for these values can be found

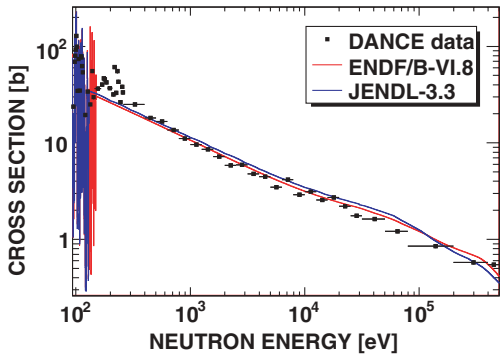

FIG. 17. (Color online) Comparison of the presently measured ^{237}Np cross sections with the data evaluations JENDL-3.3 [26], ENDF/B-VI.8 [27] in the unresolved energy region.

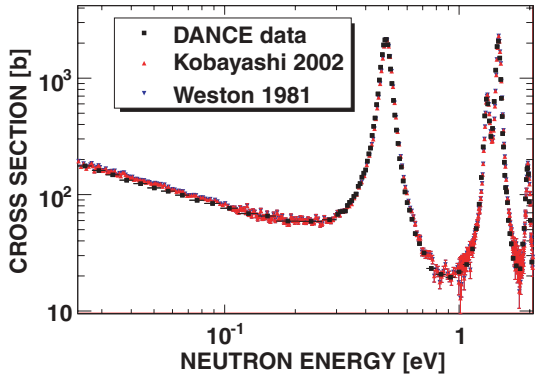

FIG. 18. (Color online) Comparison of the presently measured ^{237}Np cross sections with experimental TOF data from [29] and [10] in the thermal region.

at [2,3]. Our derived thermal value is between the very low JENDL-3.3 estimate (161.7 barn) [26] and the ENDF/B-VI.8 estimate (181 barn) [27], but is very close to the recommended value by Mughabghab (175.9±2.9 barn) [30]. The trend to low values of the thermal cross section seen by thermal activation experiments can partly be attributed to an outdated value for the γ-ray intensity of the 984 keV line in the decay of ^{238}Np. The TOF experiments tend to support higher values [10,11].

V. MODEL CALCULATIONS

We performed model calculations of the ^{237}Np neutron capture cross section for the high-energy (continuum) region using the code CoH [31]. This code uses Hauser-Feshbach statistical theory with a width-fluctuation correction by Moldauer [32]. Moldauer proposed an estimate of the channel degree-of-freedom parameter by using the Monte Carlo technique, and this was refined by Ernebjerg and Herman [33] recently, which was adopted in this study.

Neutron capture cross sections in the keV energy range are sensitive to the optical potential that determines the total compound cross section, and the ratio $\langle\Gamma_\gamma\rangle/D_0$ that is used to renormalize the γ-ray transmission coefficients, where $\langle\Gamma_\gamma\rangle$ is the averaged γ-ray width and D_0 is the averaged s-wave

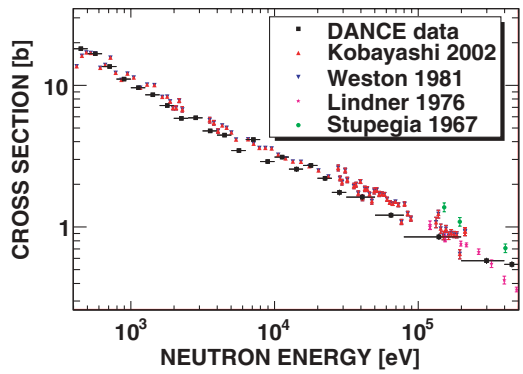

FIG. 19. (Color online) Comparison of the presently measured ^{237}Np cross sections with other experimental data in the unresolved energy region [4,5,10,29].

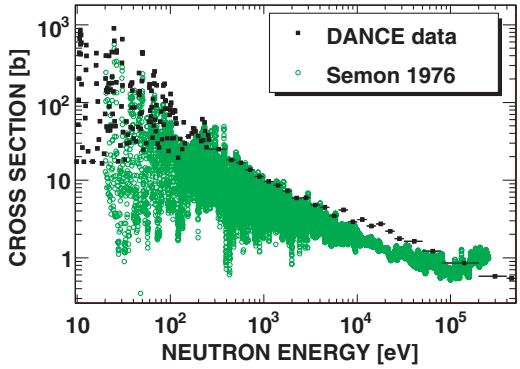

FIG. 20. (Color online) Comparison of the presently measured ^{237}Np cross sections with the only single-shot experiment using Moxon-Rae detectors [9]. In order to make this plot more readable, we chose not to show the rather large uncertainties of the Semon *et al.* data.

resonance spacing. The capture cross section is not so sensitive to the level density of ^{238}Np, when the γ-ray transmission coefficients are renormalized to the $\langle\Gamma_\gamma\rangle$ value. The level densities are calculated with a systematic study of Kawano, Chiba, and Koura [34].

The neutron transmission coefficients are calculated with the coupled-channels theory. We started with the regional coupled-channels potential parameters by Soukhovitskiĭ *et al.* [35], which were fitted to the experimental data of uranium and plutonium isotopes. Four ground-state rotational band levels, $5/2^+ - 7/2^+ - 9/2^+ - 11/2^+$, are coupled. The potential parameters were slightly modified to reproduce the experimental total cross section of Auchampaugh *et al.* [36] and Kornilov *et al.* [37], and the strength functions for s- and p-waves. We found that deformation parameters, $\beta_2 = 0.205$ and $\beta_4 = 0.06$, together with a constant optical-model imaginary surface term of $W_D = 2.59$ MeV at the low neutron incident energies ($E_n \leqslant 1.1$ MeV), give a reasonable agreement with the observable quantities. The calculated neutron strength functions are $S_0 = 0.97 \times 10^{-4}$ and $S_1 = 2.1 \times 10^{-4}$, which are compared with the evaluated values $S_0 = (1.02 \pm 0.06) \times 10^{-4}$ and $S_1 = (2.0 \pm 0.2) \times 10^{-4}$ [38]. Figure 21 shows a

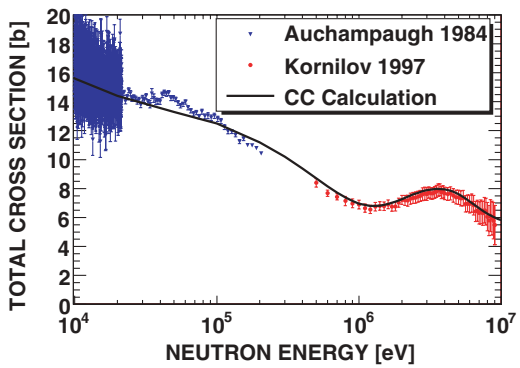

FIG. 21. (Color online) Comparison of the calculated total cross sections (coupled channels) with the experimental data of Auchampaugh *et al.* [36] and Kornilov *et al.* [37].

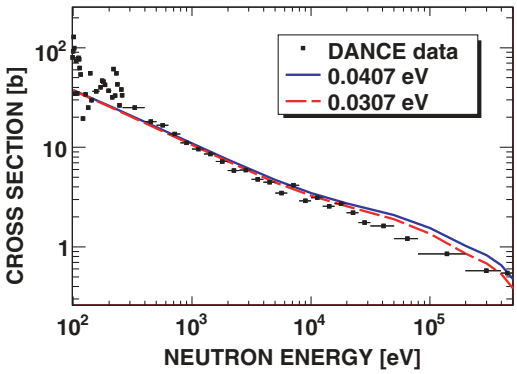

FIG. 22. (Color online) Comparison of the calculated capture cross sections with the present experimental data. The solid curve is the result of statistical model calculation with $\langle\Gamma_\gamma\rangle = 0.0407$ eV, and the dashed curve is for $\langle\Gamma_\gamma\rangle = 0.0312$ eV.

comparison of the calculated total cross sections with the experimental data.

The averaged s-wave resonance spacing D_0 and the averaged γ-ray width $\langle\Gamma_\gamma\rangle$ are taken to be 0.52 eV and 0.0407 eV, respectively [38]. The calculated capture cross sections shown as the solid curve are compared with the current experimental data in Fig. 22. The calculation is not adjusted to any experimental data, and the results shown by the dashed line in Fig. 22 agree with the experimental data of Weston and Todd [10]. Our experimental data are slightly lower than the calculated cross sections, and the calculation with $\langle\Gamma_\gamma\rangle = 0.0312$ eV agrees very well with the DANCE data.

The uncertainty in the calculated capture cross sections in the 10–100 keV range is mainly from the $\langle\Gamma_\gamma\rangle$ value adopted. Our estimation for $\langle\Gamma_\gamma\rangle$ differs from the value in [38] by 23%, and this reduction gives about 20% reduction in the calculated capture cross section in the 100 keV range. Therefore the model calculations have uncertainties of about 20% in the high-energy region.

VI. SUMMARY

In summary, the neutron capture cross section of ^{237}Np has been measured in the energy range from 20 meV to 500 keV using only 0.42 mg of ^{237}Np. Neutron capture events were detected using the Detector for Advanced Neutron Capture Experiments (DANCE), a highly segmented, 4π array of BaF_2 crystals. DANCE has a detection efficiency of about 90% for γ-rays following a neutron capture. It is therefore possible to distinguish between neutron captures on different isotopes by gating on different region in the sum energy spectrum, which allows the determination of background due to capture of scattered neutrons in the detector materials. The data are in good agreement with newer time-of-flight measurements and are in agreement with a higher value for the thermal neutron capture cross section. Our experimental data were complemented with the Hauser-Feshbach-Moldauer statistical model in the energy range from 100 eV to 1 MeV. The averaged γ-ray width of 0.0312 eV yields a good fit to the data.

ACKNOWLEDGMENTS

This work has benefited from the use of the Los Alamos Neutron Science Center at the Los Alamos National Laboratory. This facility is funded by the US Department of Energy and operated by Los Alamos National Security, LLC under contract DE-AC52-06NA25396. The Colorado School of Mines group is funded via DOE grant: DE-FG02-93ER40789.

[1] G. Aliberti, G. Palmiotti, M. Salvatores, T. K. Kim, T. A. Taiwo, M. Anitescu, I. Kodeli, E. Sartori, J. C. Bosq, and J. Tommasi, Ann. Nucl. Energy **33**, 700 (2006).
[2] K. Kobayashi, A. Yamanaka, and I. Kimura, J. Nucl. Sci. Technol. **31**, 139 (1994).
[3] T. Katoh, S. Nakamura, K. Furutaka, H. Harada, K. Fujiwara, T. Fujii, and H. Yamana, J. Nucl. Sci. Technol. **40**, 559 (2003).
[4] D. C. Stupegia, M. Schmidt, and C. R. Keedy, Nucl. Sci. Eng. **29**, 218 (1967).
[5] M. Lindner, R. J. Nagle, and J. H. Landrum, Nucl. Sci. Eng. **59**, 381 (1976).
[6] Y. E. Titarenko, O. V. Shvedov, M. M. Igumnov, E. I. Karpikhin, V. F. Batyaev, V. I. Volk, A. Y. Vakhlushin, S. V. Shepelkov, A. V. Lopatkin, S. G. Mashnik *et al.*, Nucl. Sci. Eng. **131**, 96 (1999).
[7] N. N. Buleeva, A. N. Davletshin, A. O. Tipunkov, S. V. Tikhonov, and V. A. Tolstikov, Atom. Energ. **65**, 348 (1988).
[8] A. N. Davletshin, A. O. Tipunkov, S. V. Tikhonov, and V. A. Tolstikov, Atom. Energ. **58**, 183 (1985).
[9] M. Semon, M. Hoffman, and W. Sandres, Bull. Am. Phys. Soc. **21**, 655 (1976).
[10] L. W. Weston and J. H. Todd, Nucl. Sci. Eng. **79**, 184 (1981).
[11] O. Shcherbakov, K. Furutaka, S. Nakamura, H. Sakane, K. Kobayashi, S. Yamamoto, J.-I. Hori, and H. Harada, J. Nucl. Sci. Technol. **42**, 135 (2005).
[12] F. Corvi, F. Gunsing, C. Bastian, A. Brusegan, N. Herault, J. Gonzalez, V. Gressier, A. Lepretre, E. Macavero, C. Mounier *et al.*, J. Nucl. Sci. Technol. **2**, 1067 (2002).
[13] L. Mewissen, F. Poortmans, E. Cornelis, G. Vanpraet, A. Angeletti, G. Rohr, and H. Weigmann, Nucl. Sci. Eng. **70**, 155 (1979).
[14] D. Cano-Ott, U. Abbondanno, G. Aerts, H. Alvarez, F. Alvarez-Velarde, S. Andriamonje, J. Andrzejewski, P. Assimakopoulos, L. Audouin, G. Badurek *et al.*, AIP Conf. Proc. **769**, 1442 (2005).
[15] P. W. Lisowski, C. D. Bowman, G. J. Russell, and S. A. Wender, Nucl. Sci. Eng. **106**, 208 (1990).
[16] M. Heil, R. Reifarth, M. M. Fowler, R. C. Haight, F. Käppeler, R. S. Rundberg, E. H. Seabury, J. L. Ullmann, J. B. Wilhelmy, K. Wisshak *et al.*, Nucl. Instrum. Methods A **459**, 229 (2001).
[17] D. Habs, F. S. Stephens, and R. M. Diamond, Tech. Rep., Report LBL-8945, Lawrence Berkeley Laboratory (1979).
[18] R. Reifarth, T. A. Bredeweg, A. Alpizar-Vicente, J. C. Browne, E.-I. Esch, U. Greife, R. C. Haight, R. Hatarik, A. Kronenberg, J. M. O'Donnell *et al.*, Nucl. Instrum. Methods A **531**, 528 (2004).

[19] J. L. Ullmann, U. Agvaanluvsan, A. Alpizar-Vicente, E. Bond, T. A. Bredeweg, E.-I. Esch, C. M. Folden, U. Greife, R. Hatarik, R. C. Haight *et al*., AIP Conf. Proc. **769**, 918 (2005).
[20] N. Talavitie, Anal. Chem. **44**, 280 (1972).
[21] E.-I. Esch and R. Reifarth, Technical Report LA-UR-03-5560, Los Alamos National Laboratory (2003).
[22] A. F. Mertz, T. A. Bredeweg, A. Couture, M. Jandel, R. C. Haight, J. M. O'Donnell, R. Reifarth, R. S. Rundberg, J. R. Tesmer, J. L. Ullmann *et al*., Technical Report LA-UR-06-7232, Los Alamos National Laboratory (2006).
[23] J. Apostolakis, Technical Report, CERN, GEANT library (1993), http://wwwinfo.cern.ch/asd/geant/.
[24] R. Brun and F. Rademakers, Nucl. Instrum. Methods A **389**, 81 (1997).
[25] R. B. Firestone, *Table of Isotopes* (Wiley, New York, 1996).
[26] K. Shibata, T. Kawano, T. Nakagawa, O. Iwamoto, J. Katakura, T. Fukahori, S. Chiba, A. Hasegawa, T. Murata, H. Matsunobu *et al*., J. Nucl. Sci. Technol. **39**, 1125 (2002).
[27] ENDF-LIBRARY, Technical Report, National Nuclear Data Center, On-Line Access: www.nndc.bnl.gov/nndc/endf/; Brookhaven National Laboratory (2001).
[28] See EPAPS Document No. E-PRVCAN-77-050803 for Differential Neutron Capture Data for ^{237}Np. For more information on EPAPS, see http://www.aip.org/pubservs/epaps.html.
[29] K. Kobayashi, S. Lee, S. Yamamoto, H. J. Cho, and Y. Fujita, J. Nucl. Sci. Technol. **39**, 111 (2002).
[30] S. Mughabghab, *Neutron Cross Sections* (Academic Press, New York, 1984), Vol. 1, Part B.
[31] T. Kawano, S. Chiba, T. Maruyama, Y. Utsuno, H. Koura, and A. Seki, in *Proceedings of the 2003 Symposium on Nuclear Data, 27–28 Nov., 2003, JAERI, Tokai, Japan, 2004* (JAERI, Tokai, 2004).
[32] P. A. Moldauer, Nucl. Phys. **A344**, 185 (1980).
[33] M. Ernebjerg and M. Herman, AIP Conf. Proc. **769**, 1233 (2005).
[34] T. Kawano, S. Chiba, and H. Koura, J. Nucl. Sci. Technol. **43**, 1 (2006).
[35] E. S. Soukhovitskii, S. Chiba, J. Y. Lee, O. Iwamoto, and T. Fukahori, J. Phys. G: Nucl. Part. Phys. **30**, 905 (2004).
[36] G. F. Auchampaugh, M. S. Moore, J. D. Moses, R. O. Nelson, R. C. Extermann, C. E. Olsen, N. W. Hill, and J. A. Harvey, Phys. Rev. C **29**, 174 (1984).
[37] N. V. Kornilov, A. B. Kagalenko, V. Y. Baryba, V. G. Demenkov, S. V. Pupko, and P. A. Androsenko, Ann. Nucl. Energy **27**, 1643 (2000).
[38] S. Mughabghab, *Atlas of Neutron Resonances, Resonance Parameters and Thermal Cross Sections, Z = 1–100* (Elsevier, New York, 2006).